Jurnal Kejuruteraan 36(4) 2024: 1689–1697
https://doi.org/10.17576/jkukm-2024-36(4)-31

Performance of GFRP Sheets in Strengthening Concrete Beams in Flexure

Sakhiah Abdul Kudus[a,b*], Siti Hajar Aisyah Mohd Din[a], M. S. Haji Sheik Mohammed[c], V. Roopac & Zakiah Ahmad[a,b]

[a]*School of Civil Engineering, Universiti Teknologi MARA (UiTM), 40450 Shah Alam, Malaysia*

[b]*Institute for Infrastructure Engineering and Sustainable Management (IIESM),*

Universiti Teknologi MARA, 40450 Shah Alam, Selangor, Malaysia

[c]*Department of Civil Engineering, B.S. Abdur Rahman Crescent Institute of Science and Technology, Chennai 600 048, India*

[*]*Corresponding author: sakhiah@uitm.edu.my*

Received 1 March 2024, Received in revised form 9 May 2024
Accepted 9 June 2024, Available online 30 July 2024

ABSTRACT

Plain concrete beam repair and strengthening are increasingly important in structural strengthening and retrofitting. This study examines the glass fibre-reinforced polymer (GFRP) sheets in plain concrete beams under flexural behaviour by using its patching sheets. Through the implementation of a symmetrical four-point static loading technique, a series of tests were conducted on plain concrete beams that had been externally joined with GFRP sheets. These beams were subjected to rigorous testing until they reached their ultimate failure point. The experimental test consists of casting nine plain concrete beams with identical specifications. Three beams are utilised as control beams; three are reinforced with GFRP sheets measuring 50 mm × 100 mm, and another three are reinforced with GFRP sheets measuring 100 mm × 200 mm. The flexural test is designed to determine the tensile strength of concrete under bending. Compared to the control beams, the specimens strengthened with GFRP sheets demonstrated a significantly enhanced ultimate load capacity. The beams with larger GFRP sheets exhibited a higher ultimate load of 14.84 kN, while those with smaller sheets showed an ultimate load of 8.54 kN, marking an appreciable improvement in performance. Moreover, the smaller area GFRP-reinforced beams failed at a 45% higher shear stress compared to those with a larger area GFRP, indicating a differential impact based on the size of the reinforcement used. This study highlights the effectiveness of GFRP sheets in enhancing the structural performance of plain concrete beams, providing crucial insights into the benefits of different sizes of reinforcement.

Keywords: Glass fiber reinforced polymer (GFRP) sheet; Concrete beam; Strengthening; Ultimate load; Energy absorption.

INTRODUCTION

Reinforcing existing concrete structural components has emerged as a highly desirable effort in civil engineering. Upgrading current structures is an essential component of structural engineering practice that necessitates a particular solution. Concrete structural rehabilitation and repair can reinstate any deteriorated or damaged structure, extending the structure's longevity and load-carrying capacity. Concerns about reinforcing the concrete structure initially appeared when its original function or purpose was altered. The structure alteration refers to strengthening occurrence. A four-point bending test is used to bend the material and measure stress at the failure point. The tests distribute the maximal flexural stress across the beam section bounded by the loading points. According to Gopu and Sofi (2022), concrete beams break under flexural testing. However, various loads can deteriorate the structure's efficiency and strength, causing the components to crack and bend. According to Jabbar and Farid (2018), by using a GFRP sheet, structural cracks and bends can be decreased during flexural testing.

According to Soudki et al. (2002), cracks in concrete structures often appear when the material's tensile strength is exceeded and spread perpendicular to its maximum stress. Shear stress and ultimate load are usually the causes of concrete structural failure. Fiber-reinforced polymers possess enhanced characteristics, including a remarkable strength-to-weight ratio, excellent stiffness-to-weight ratio, resistance to corrosion, versatile design options, outstanding durability, and straightforward execution methods. For the flexural integrity of the beam, fiber-reinforced polymer sheets or plates adhere to the tension face of a member or its bottom face in the case of a merely supported member with applied top loading or gravity loading (Choobbor et al., 2019; Dong et al., 2013). The primary tensile fibres of the structure are oriented along the longitudinal axis, just like the internal flexural of the beam. Even though the beam's deflection capacity and flexibility are reduced, its strength and stiffness (the load needed to induce unit deflection) are increased.

The previous research conducted by Dong et al. (2013) focused on concrete pillars reinforced with carbon and glass fiber-reinforced polymer (FRP) sheets for external flexural and flexural-shear purposes. The re-search investigated retrofitted concrete beams' flexural and flexural shear strengthening capabilities.

Additionally, it demonstrated the impact of different strengthening configurations utilising CFRP and GFRP sheets on the post-strengthened behaviour of the concrete beams. The findings suggest that the flexural shear reinforcement concept is considerably more effective than the flexural one when enhancing the concrete beam's rigidity, ultimate strength, and hardening characteristics,

Recent research indicates that carbon fiber-reinforced polymer (CFRP) composites are predominantly and effectively utilised to strengthen concrete beams flexibly (Hawileh et al., 2022). This study compares the reliability of concrete beams reinforced with high-density (HSM) and medium-density (MSM) laminates to CFRP laminates. In addition to the two unstrengthened control beam specimens, six concrete beams were reinforced in flexure with comparable CFRP, MSM, and HSM laminates. Testing was conducted on all beam specimens to evaluate symmetrical monotonic loading. Strain data and midspan deflection were carefully recorded during the experiments. Based on experimental data, HSM laminates outperformed CFRP and MSM laminates in terms of concrete beam stiffness, energy absorption, flexural strength, cracking performance, and flexibility. Recent studies further validate the growing interest in GFRP for concrete reinforcement. Tharmarajah, Taylor, and Robinson (2023) explored the compressive membrane action in GFRP-reinforced concrete slabs, highlighting the necessity for design adjustments in GFRP applications due to their distinct mechanical behaviors compared to traditional reinforcements (Tharmarajah et al., 2023). Additionally, Hassanpour and Kinjawadekar (2023) discussed the flexural behavior of concrete beams reinforced with GFRP bars, emphasizing their superior performance in terms of load capacity and sustainability, particularly in aggressive environments where durability is crucial (Hassanpour & Kinjawadekar, 2023).

Moreover, a study by Choobbor et al. (2019) delves into the bending behaviour in concrete beams reinforced with sheet composites made of carbon and basalt fibre-reinforced polymer (CFRP/BFRP). The proposed hybrid systems enhance strengthening composite material properties, including tensile BFRP sheets adhered to high-strength CFRP sheets using epoxy glue. A total of ten beams were examined; nine underwent reinforcement with different CFRP and BFRP sheet combinations, and the tenth beam served as a control specimen. The results of the tests indicated that the load-bearing capacity and elasticity of the reinforced specimens were significantly improved.

Galal and Mofidi (2009) propose a novel system for rehabilitating concrete beams, consisting of a hybrid fiber-reinforced polymer FRP sheet and ductile anchor. The suggested strengthening method offers a solution to the issue of poor flexibility commonly associated with brittle failure modes, unlike traditional methods that rely on epoxy-bonded FRP sheets. The suggested method triggers bending in steel anchor system steel connections rather than the immediate rupture or debonding of FRP sheets. Four T-beams made of concrete were tested using a four-point bending method. Using a single layer of carbon FRP sheet, three beams were reinforced through retrofitting. A comparison was made between the outcomes of two beams reinforced with the novel hybrid FRP sheet/ductile anchor system and the control beam and the beam strengthened with the conventional FRP bonding approach. Despite extensive research in the field of structural strengthening, significant gaps remain, particularly in understanding the practical application of reinforcement materials under varied environmental conditions. Many studies focus predominantly on immediate structural enhancements and often overlook detailed evaluations of energy absorption capabilities and damage patterns related to the bonding of reinforcement materials like Glass Fiber Reinforced Polymer (GFRP). This study addresses these gaps by assessing not only the immediate flexural strength improvements but also exploring how GFRP improves energy absorption and influences damage patterns within concrete structures.

This experimental study aims to analyse the performance of glass fibre-reinforced plastic (GFRP) sheets in reinforced concrete beams in flexure. It involves an assessment of the flexural behaviour of plain concrete

beams using patched GFRP sheets. Externally linked plain concrete beams reinforced with GFRP sheets were tested for failure using a symmetrical four-point static loading approach. The experimental test consists of the casting of nine plain concrete beams. All cast beams share identical characteristics and exhibit a weakness in flexural strength. Three beams are utilised as control beams, three beams are reinforced using GFRP sheets measuring 50 mm × 100 mm, and another three beams are reinforced using GFRP sheets measuring 100 mm × 200 mm. The flexural test determines the tensile strength of concrete under bending. Prism specimens underwent four-point bending testing, and the bond strength was calculated using the elastic mechanics approach based on the load-carrying capacity of the tested prisms. Furthermore, the experimental configuration and dimensions of the specimen adhered to the guidelines outlined in BS EN 12390-5:2009 for design purposes. The outcomes are beneficial and boost the confidence of related parties in applying the GFRP sheet to reinforce concrete structures.

EXPERIMENTAL PROGRAM

This study used a specific concrete mixture to create concrete cubes and beams. The beam's design adhered to the specifications outlined in British Standard (BS) 8110: Part 1:1985, with dimensions of 100 mm width, 100 mm height, and 500 mm length. The dry and clean local river sand was utilised as the fine aggregate. Based on British Standard BS 882:1992, crushed stone produced the coarse aggregate with a maximum particle size of 20 mm. A particle size of 10 mm was selected due to its prevalence in practical applications (BS 882, 1992). A particle size of 10 mm was selected due to its prevalence in practical applications. A 4.75 mm sieve was employed to separate the sand, as this dimension is suitable for passing fine aggregate. After the sieving process, the density of the material is multiplied by the amount of concrete that needs to be cast that day to determine the weight of the water, cement, fine aggregate, and coarse aggregate. After adding water, the concrete is thoroughly mixed in the drum for a minimum duration of two minutes. Any segregation in the concrete is blended back into the mixture once it has been withdrawn from the mixer. Compressive strength tests were conducted to ascertain the concrete's strength. The concrete beam was cast using a flashboard in the sample production process. During the casting process, the vibrator is utilised for compacting. The formwork was removed following 24 hours, and the specimen was immersed in water and left to cure for 28 days. Following the curing process, a saw-cutting table machine fabricated the notched-on beam. The required size and position were tagged and marked before cutting the item.

STRENGTHENING PROCEDURE SETUP

The sizes indicated for the beam tests complied with the requirements of the International Union of Laboratories and Experts in Construction Materials, Systems, and Structure (RILEM) in 1990. It is recommended to have a notch gap width of approximately 1 to 3 mm. The notch length must not surpass half the height of the specimen, ensuring that the maximal notch-to-depth ratio does not exceed 0.5. The GFRP sheet was applied following the procedure specified by the manufacturer. The surface preparations of the GFRP were determined following the guidelines of ACI 440.9R-15.

Table 1 displays the specific dimensions of the GFRP sheet. An electric disc sander was used to smooth the bottom surfaces of the beams before the GFRP sheet was installed. The standard choice was the epoxy resin Sikadur-31CF, used (Omar et al., 2023). Two ingredients are needed for this thixotropic epoxy adhesive, Parts A and B, which should be mixed in a 2:1 ratio. The GFRP sheet was placed on the table, and the epoxy resin was applied using a soft roller to impregnate all the fibres. Figure 1 depicts the specimen covered in GFRP sheeting. Following that, the specimen was coated with a white colour. Subsequently, a ruler was used to compose a grid of squares measuring approximately 25 mm by 25 mm, corresponding to the specimen's dimensions.

TABLE 1. Details size of GFRP sheet

Specimen	Width of GFRP sheet (mm)	Length of GFRP sheet (mm)
GFRPS-50	50	100
GFRPS-100	100	200

(a) 50mm sheet (b) 100mm sheet

FIGURE 1. Specimen with GFRP sheet

FLEXURAL TEST

Specimens were equipped with strain gauges before the flexural testing. By brushing the surface, stray particles

and a thin layer of cement were eliminated, thereby revealing the textured, smooth surface of the concrete. The mechanical assessment was performed using four-point bending tests on actual, supported beams. The deflection and loading were measured using LVDTs with a load cell. According to Hawileh et al. (2022), the studies were carried out under displacement control with a constant displacement rate of 0.2 mm/min. Every specimen was subjected to four-point bending tests with a 300 mm span until they failed. The supporting rollers were positioned at an equal distance of 100 mm from the two focal loads. The mid-span deflection was measured using a linear variable displacement transducer (LVDT). The specimen dimensions and test configuration adhered to the guidelines specified in BS EN 12390-5:2009. In addition to observing and computing the failure modes, the ultimate reached shear (bond) strength and load-carrying capacity were also assessed. Figure 2 shows the four-point bending tests applied throughout the study.

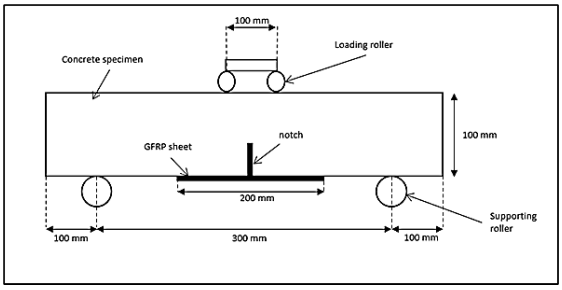

(a) Schematic diagram of the setup

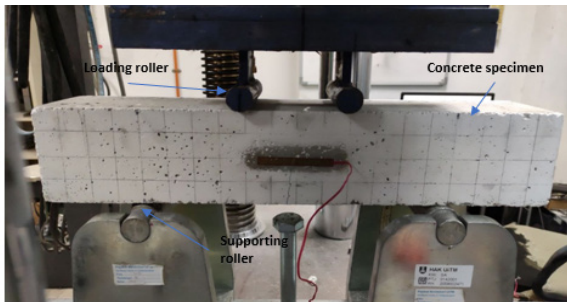

(b) Complete setup of testing

FIGURE 2. Setup of the instrument for four-point load test

RESULTS AND DISCUSSION

WORKABILITY TEST

The mix's functionality was assessed by conducting a slump test. A slump test is run, and a visual comparison is made using only the naked eye prior to pouring the concrete into the mould. The concrete slump test assesses the consistency of fresh concrete before its hardening. It serves to determine the level of workability and the flowability of freshly mixed concrete. This study's average slump test value of 32 mm (Table 2) highlights the significance of this method in evaluating the consistency and flow properties of fresh concrete (American Concrete Institute, 2016).

TABLE 2. Slump test value

Sample	Slump Value (mm)
1	32
2	31
3	35

COMPRESSIVE TEST

Compression testing can assess a material's plastic flow behaviour, elasticity fracture limits, and response to crushing loads. The purpose is to determine the strength of the concrete and ensure that it achieves a minimum of 3 N/mm2 after 28 days of curing. Table 3 displays the outcomes of the concrete compressive strength for all specimens. The objective of these tests was to evaluate the ability of the concrete to reach the desired strength of 30 N/mm² by day 28 of curing, which is critical for ensuring the structural integrity and durability of the concrete beams. The data presented in Table 3 show that by the 28th day, the compressive strength of all samples ranged from 48.66 N/mm² to 49.44 N/mm². These results not only demonstrate that our concrete mix successfully achieved the desired strength threshold but also consistently exceeded it across all tested samples.

Four-point bending tests were conducted on real, supported beams to evaluate their mechanical properties. The flexural stress in these tests showed a gradual increase of 0.0033 mm/s under displacement control. At 300 mm, each specimen underwent four-point bending testing until failure. The tensile strength of the specimen was determined through the static test; this value was then correlated with the maximum load capacity of each variety of notched beams. The specimen would subsequently fracture completely. The ultimate or maximal load is a crucial metric for estimating the specimen's failure load during testing.

TABLE 3. Results of concrete compressive strength of all specimens

Day	Sample	Maximum load (kN)	Compressive Stress (N/mm^2)	Compressive Stress (N/mm2)
7 day	1	382.51	38.25	39.19
	2	402.94	40.29	
	3	390.37	39.04	
14 day	1	438.85	43.88	44.82
	2	427.36	42.74	
	3	478.27	47.83	
21 day	1	373.50	37.35	43.57
	2	476.00	47.46	
	3	459.08	45.91	
28 day	1	491.34	49.13	49.08
	2	494.42	49.44	
	3	486.60	48.66	

ULTIMATE LOAD CAPACITY

The GFRPS-100 beam with a notch and a GFRP sheet size of 100 mm × 200 mm achieved the highest recorded value of 14.84 kN in the static flexural test. Then, GFRP-50 with a notch and a GFRP sheet size of 50 mm × 100 mm has a force of 8.54 kN. The control beam with a notch and without the GFRP sheet exhibits the lowest ultimate load, measuring 5.66 kN. Table 4 displays the findings of the flexural test, including the maximum ultimate load and the percentage ultimate load over CB.

Figure 3 exhibits the ultimate load-carrying ca-pacity and percentage augmentation. The strengthened specimens showed a significant increase in ultimate load-carrying capacity compared to the control beam. Specifically, specimens GFRPS-50 and GFRPS-100 exhib-ited a 34% and 62% increase, respectively. Specimens reinforced with a larger area of GFRP sheet demonstrat-ed a higher ultimate load of 14.84 kN, in contrast to spec-imens reinforced with a smaller area of GFRP sheet with an ultimate load of 8.54 kN.

TABLE 4. Maximum static load for each type of specimen

	Beam 2	Beam 3	Average P_{ult} (kN)	% P_{ult} increase over CB (%)
CB	5.77	5.75	5.46	5.66	-
GFRPS-50	6.73	8.83	10.08	8.54	34
GFRPS-100	13.29	14.53	16.69	14.84	62

ULTIMATE LOAD CAPACITY

Figure 4 displays the load-deflection curves obtained from the experiments on the CB, GFRPS-50, and GFRPS-100 specimens. The CB was used as a benchmark for comparing the specimen's performance that had been supplemented with the GFRP sheet. The control and enhanced specimens have trilinear load-deflection curves, which can be described in three phases. All beam specimens in the initial stage exhibit identical stiffnesses as no flexural cracks have developed yet. The condition may be due to the rigidity of the beam and the overall moment of inertia of the undamaged section. During the second stage, the specimens display different stiffnesses due to the formation of small flexural cracks near the midspan of the beam. This is because the effective reinforcement ratio influences the stiffness of each specimen. During the initial phase of the flexural fractures, the stiffness of the beams was affected. The load-deflection curves indicated decreased slopes during this particular loading stage. The reinforced beams endured failure at lower deflection values compared to the CB specimens. The flexure crack emerged in the mid-span and its surrounding area.

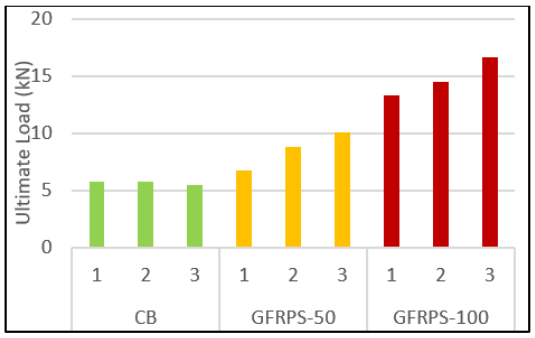

FIGURE 3. Percentage enhancement and ultimate load-carrying capacity specimens

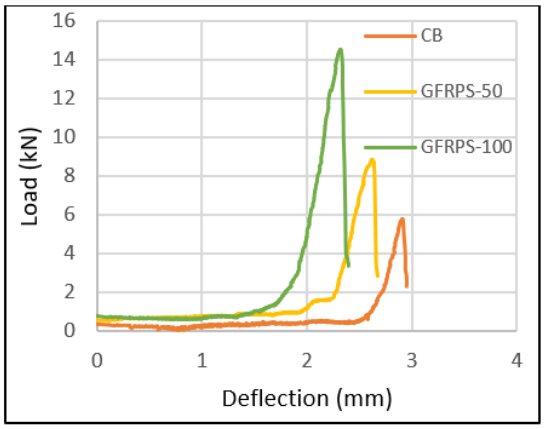

FIGURE 4. Load versus midspan deflection

ENERGY ABSORPTION

Understanding the fracture mechanism of specimens relies heavily on analysing their energy absorption. Thus, the energy absorption was calculated using the area under the load-deflection response curves. Energy absorption is a fundamental feature that is essential in comprehending specimen fracture mechanisms. Table 5 displays the energy absorption values for all the tested specimens. The GFRPS-50 and GFRPS-100 specimens showed a 70% and 45% percentage increase in energy absorption over the CB specimen, respectively. The outcomes show that specimen CB exhibited the lowest energy absorption while specimen GFRPS-100 demonstrated the highest. Figure 5 highlights the percentage enhancement and energy absorption capacity of the specimens.

TABLE 5. Energy absorption capacity of control and strengthened specimens

Test Specimen	Energy Absorption (kN.mm)	Increase over CB (%)
CB	2.185	-
GFRPS-50	3.964	45
GFRPS-100	7.284	70

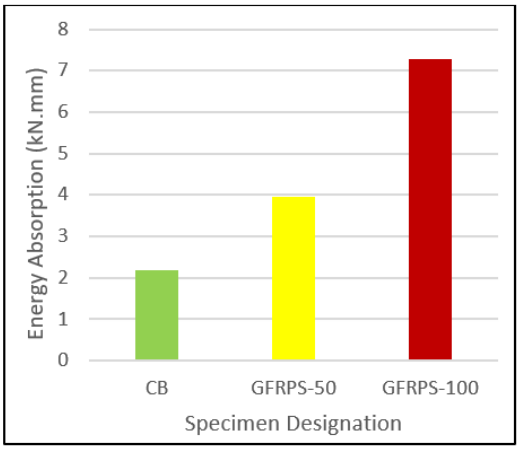

FIGURE 5. Percentage enhancement and the energy absorption capacity of specimens

LOAD-STRAIN RELATIONSHIP

Figure 6 shows the load vs strain response for the strengthened specimens at the midspan. Specimens CB, GFRP-50, and GFRP-100 exhibited ultimate strain percentages of 1.09%, 0.967%, and 0.868%, respectively. The GFRP-100 exhibits the lowest strain percentage but the highest ultimate load, while the CB specimen shows the highest strain percentage but the lowest ultimate load. Consequently, all of the reinforced specimens failed via sheet debonding and delamination (concrete cover separation) before the concrete midspan of the beam was impacted.

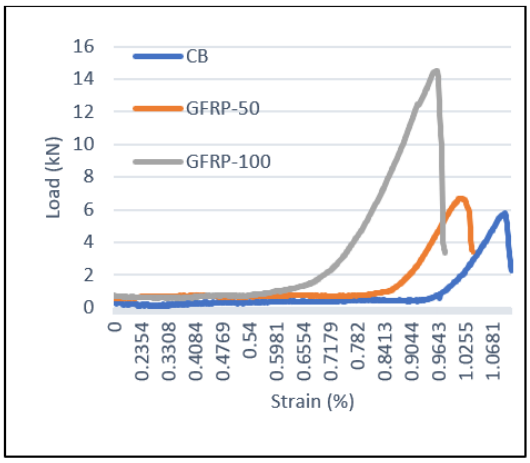

FIGURE 6. Load versus strain of the specimen

BOND STRENGTH OF PRISM SPECIMEN

Table 6 presents the bond test findings as computed ultimate shear stress (τ), ultimate load (Pu), and associated failure modes. Equation (1), which denotes the internal action of forces, was utilised to compute the ultimate shear stress of the laminates. When calculating the applied ultimate load (P), it is important to consider the length of the specimen (L), the height of the specimen (h), the width of the composite sheet (w), and the total length of the composite sheet (S).

TABLE 6. Flexural bond test results

Test Specimen	Ultimate load, P_{ult} (kN)	Shear stress, τ (Mpa)	Failure
CB1	5.77	0.866	Flexural
CB2	5.75	0.863	Flexural
CB3	5.46	0.819	Flexural
GFRPS-50-1	6.73	4.04	Adhesive
GFRPS-50-2	8.83	5.30	Adhesive
GFRPS-50-3	10.08	6.05	Adhesive
GFRPS-100-1	13.29	1.99	Interface
GFRPS-100-2	14.53	2.18	Interface
GFRPS-100-3	16.69	2.50	-

$$\tau = \frac{3PL}{5hwS} \quad (1)$$

The primary presumption for calculating shear stress using an equation is that the compression zone has a linear stress distribution over half of the specimen's height. Specimen GFRP-50 presented a higher failure point under shear stress when compared to specimen GFRP-100. Table 6 additionally shows the failure mechanism for every specimen where specimen CB exhibits a flexural failure mode. In addition, specimen GFRP-50 experienced adhesive failure, while specimen GFRP-100 encountered interface failure.

FAILURE MODE

Figure 7 illustrates the failure mode of the strengthened beam. Testing has identified multiple failure modes, such as interfacial and adhesive failures. An adhesive mode failure was detected in specimens bonded with a small section of GFRP sheet. An interfacial mode was detected in specimens reinforced with a larger surface area of the GFRP sheet. In contrast, specimen GFRP-50 cracks not at the mid-span and has an average ultimate load of 8.58 kN, while specimen GFRP-100 cracks at the mid-span of the beam and has an average ultimate load of 14.84 kN.

In a study conducted by Meikandaan & Ramachandra Murthy (2017), it was found that the strengthened beam had an ultimate load-carrying capability that was 14% higher than the regulated beam. FRP laminate enhances a beam's energy absorption, delays crack formation and enhances load-carrying capacity. When the 70% damaged beams are reinforced with a 100 mm wide by 1.2 mm thick GFRP sheet for the bottom full, their load-carrying capability increases by 14% compared to the control beam. A study by Hawileh et al. (2022) suggests that specimens reinforced with CFRP laminate commonly exhibited a debonding failure mode. Nevertheless, the beams reinforced with MSM and HSM laminates failed due to concrete cover separation (delamination). Concrete beams reinforced with HSM laminates outperform their CFRP and MSM counterparts in strength, stiffness, flexural bond strength, and elasticity. The ultimate load-carrying capacity of CFRP, MSM, and HSM showed a significant increase of 58%, 55%, and 65%, respectively, when compared to the control specimens. The HSM laminated specimens showed superior energy absorption and deflection compared to other strengthened specimens. The beam improved with the HSM laminates showed greater ultimate and failure ductility values than the beams strengthened with CFRP and MSM laminates. The failure elasticity for HSM samples was between 23.4% and 34.5% higher than for CFRP and MSM laminates. The shear tension at which the concrete beam specimen bonded with HSM failed was greater than those bonded with CFRP and MSM. The ultimate shear stress varied between 7% and 23% for the CFRP and MSM-bonded and HSM-bonded specimens.

Other findings indicate that applying GFRP sheets for reinforcing concrete structures is both pragmatic and effective (Sivasankar et al., 2018). The first crack in the control beam appeared at 57.5 kN, and more cracks were seen at 70 kN. The final deflection was 298 mm, measured from the bottom of the beam. This beam's initial base height measured 340 mm. Moreover, the U-wrapping, consisting of a solitary GFRP sheet, experienced failure when subjected to an ultimate load of 114.35 kN, resulting in a deflection of 310 mm from the base of the beam, where the height was initially measured at 338 mm. Subsequently, when a beam was partially enveloped by a solitary layer of GFRP sheet at its lowermost section, it experienced a failure at a load of 109.80 kN and a deflection of approximately 310 mm at a base height of 345 mm from the bottom. The flexural strengths of U-shaped beams that contain a single layer of GFRP sheets and a double layer of sheets are 18.296 N/mm^2 and 19.712 N/mm^2, respectively.

Similarly, a partially wrapped beam with one layer of GFRP sheets has a flexural strength of 17.568 N/mm^2, while the same beam with two layers has a flexural value of 18.25 N/mm^2. The beam encased in two layers of GFRP sheets demonstrates a greater proportion of flexural strength. The percentage of flexure has doubled compared to the control beam.

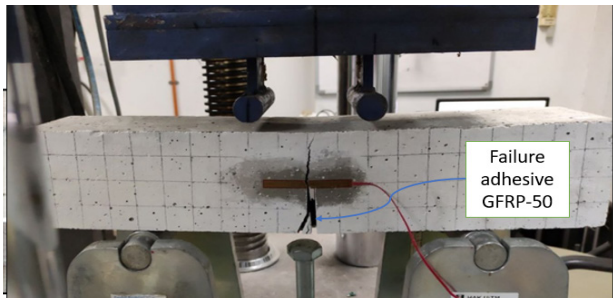

(a)

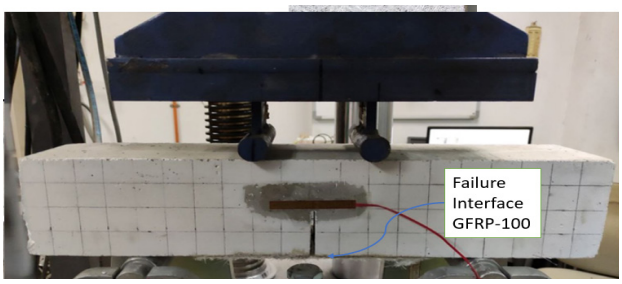

(b)

FIGURE 7. Crack pattern specimen (a) GFRP-50 and (b) GFRP-100

CONCLUSION

In conclusion, the results obtained from the four-point bending test that was performed to determine the flexural capacity of the control beam were relevant. The ultimate load capacity, the lowest for specimen CB, is not equipped with GFRP reinforcement. CB also significantly encountered failure at a comparatively elevated deflection value, suggesting its structural integrity was substandard. Moreover, the control beam exhibited the least capacity for energy absorption, highlighting its restricted resistance to external forces. CB specimens showed the highest strain percentages in conjunction with the lowest ultimate loads to indicate their susceptibility to deformation and stress.

In contrast, the evaluation of reinforced beams utilising Glass Fibre Reinforced Polymer (GFRP) sheets revealed substantial improvements in their ability to resist bending. Specimens like GFRPS-100, which had bigger dimensions of GFRP sheets, had the highest capacity to withstand loads. The addition of GFRP reinforcement resulted in a significant enhancement in the ability to withstand loads. Specifically, specimens GFRPS-50 and GFRPS-100 demonstrated 34% and 62% improvements, respectively, compared to the control beam. In addition, it was observed that reinforced beams failed at reduced deflection values, suggesting an improvement in their structural resilience. Significantly, larger regions of GFRP sheets were shown to be associated with a more rigid and fragile response, resulting in enhanced ability to absorb energy ranging from 45% to 70% compared to CB specimens. Energy absorption capabilities were also greater in beams strengthened with longer GFRP sheets.

Significant insights emerged during the bond strength study, including analysing ultimate shear stress and identifying bond failure. Beams reinforced with smaller areas of GFRP sheets demonstrated greater resistance to shear stress compared to beams with larger GFRP sheet areas and the control beam. The observed failure modes exhibited variation, with CB specimens primarily undergoing flexural failure. In contrast, specimens with lower GFRP areas displayed adhesive failure, and those with greater GFRP areas showed interfacial failure. These results highlight the complex interactions that improve structural performance and resilience between GFRP reinforcement, bond strength, and failure mechanisms.

ACKNOWLEDGEMENT

The authors would like to express their gratitude to the College of Engineering, Universiti Teknologi MARA Shah Alam, and the grant 100-TNCPI/INT 16/6/2 (058/2022).

DECLARATION OF COMPETING INTEREST

None

REFERENCES

American Concrete Institute. 2016. ACI 211.1-91, Standard Practice for Selecting Proportions for Normal, Heavyweight, and Mass Concrete (ACI 211.1-91). Farmington Hills, MI: American Concrete Institute.

American Concrete Institute. 2015. Guide to accelerated conditioning protocols for durability assessment of internal and external fiber-reinforce polymers (FRP) reinforcement. ACI 440.9R-15.

British Standard Institution. 2004. Products and systems for the protection and repair of concrete structures - Definitions, requirements, quality control and evaluation of conformity - Part 4: Structural bonding. EN1504-4:2004.

British Standard Institution. 2001. Testing hardened concrete - Part 3: Compressive strength of test specimens. BS EN 12390-3:2001

British Standard Institution. 2009. Testing hardened concrete - Part 5: Flexural Strength of Test Specimens. BS EN 12390-5:2009.

British Standards Institution. 1992. BS 882:1992, Aggregates from natural sources for concrete. London: BSI Standards Limited.

Choobbor, S. S., Hawileh, R. A., Abu-obeidah, A., & Abdalla, J. A. 2019. Performance of hybrid carbon and basalt FRP sheets in strengthening concrete beams in flexure. *Composite Structures* 227: 111337. https://doi.org/10.1016/j.compstruct.2019.111337

Dong, J., Wang, Q., & Guan, Z. 2013. Composites: Part B Structural behaviour of RC beams with external flexural and flexural – shear strengthening by FRP sheets. *Composites Part B* 44(1): 604–612.

Hawileh, R. A., Nuaimi, N. Al, Nawaz, W., Abdalla, J. A., & Sohail, M. G. 2022. Flexural and Bond Behavior of Concrete Beams Strengthened with CFRP and Galvanized Steel Mesh Laminates. 27(1): 1–14. https://doi.org/10.1061/(ASCE)SC.1943-5576.0000651

Choobbor, S. S., Hawileh, R. A., Abu-obeidah, A., & Abdalla, J. A. 2019. Performance of hybrid carbon and basalt FRP sheets in strengthening concrete beams in fl exure. *Composite Structures* 227(March): 111337. https://doi.org/10.1016/j.compstruct.2019.111337

Galal, K., & Mofidi, A. 2009. Strengthening RC beams in flexure using new hybrid frp sheet / ductile anchor system. 13(3): 217–225.

Omar, Z., Sugiman, S., & B, M. M. Y. 2023. Proceedings of the First Mandalika International Multi-Conference on Science and Engineering 2022, MIMSE 2022 (Civil and Architecture). In Proceedings of the First Mandalika International Multi-Conference on Science and Engineering 2022, MIMSE 2022 (Civil and Architecture) (Vol. 3). Atlantis Press International BV. https://doi.org/10.2991/978-94-6463-088-6

Gopu, G. N., & Sofi, A. 2022. The influence of fiber RC beams under flexure on the chloride-induced corrosion. *Case Studies in Construction Materials* 17(October): e01566. https://doi.org/10.1016/j.cscm.2022.e01566

Hassanpour, H., & Kinjawadekar, T. 2023. Flexural behaviour of reinforced concrete beams reinforced with Glass Fiber-Reinforced Polymer (GFRP) bars. *Arabian Journal for Science and Engineering.* https://link.springer.com/article/10.1007/s13369-023-07540-3

Jabbar, S. A. A., & Farid, S. B. H. 2018. Replacement of steel rebars by GFRP rebars in the concrete structures. *Karbala International Journal of Modern Science* 4(2): 216–227. https://doi.org/10.1016/j.kijoms.2018.02.002

Meikandaan, T. P., & Ramachandra Murthy, A. 2017. Flexural behaviour of RC beam wrapped with GFRP sheets. *International Journal of Civil Engineering and Technology* 8(2): 452–469.

Sivasankar, S., Bharathy, T., & Vinodh Kumar, R. 2018. Flexural behaviour of RC beams using GFRP composites. *International Journal of Engineering & Technology* 7(3.12): 744. https://doi.org/10.14419/ijet.v7i3.12.16493

Soudki, K. A, Sherwood, T., & Masoud, S. 2002. FRP repair of corrosion-damaged reinforced concrete beams. Proceedings of the 3rd Fib International Congress – 2010, 1–13. http://quakewrap.com/frp papers/FRP-Repair-of-Corrosion-Damaged-Reinforced-Concrete-Beams.pdf

Tharmarajah, G., Taylor, S., & Robinson, D. 2023. Experimental and numerical investigation of compressive membrane action in GFRP-reinforced concrete slabs. *Polymers* 15(5): 1230. https://doi.org/10.3390/polym15051230